ACS APPLIED MATERIALS & INTERFACES

www.acsami.org

Research Article

Magnetic Nanoparticles as a Tool for Remote DNA Manipulations at a Single-Molecule Level

Aleksey A. Nikitin,* Anton Yu Yurenya, Timofei S. Zatsepin, Ilya O. Aparin, Vladimir P. Chekhonin, Alexander G. Majouga, Michael Farle, Ulf Wiedwald, and Maxim A. Abakumov*

Cite This: *ACS Appl. Mater. Interfaces* 2021, 13, 14458−14469

Read Online

ACCESS | Metrics & More | Article Recommendations | Supporting Information

ABSTRACT: Remote control of cells and single molecules by magnetic nanoparticles in nonheating external magnetic fields is a perspective approach for many applications such as cancer treatment and enzyme activity regulation. However, the possibility and mechanisms of direct effects of small individual magnetic nanoparticles on such processes in magneto-mechanical experiments still remain unclear. In this work, we have shown remote-controlled mechanical dissociation of short DNA duplexes (18−60 bp) under the influence of nonheating low-frequency alternating magnetic fields using individual 11 nm magnetic nanoparticles. The developed technique allows (1) simultaneous manipulation of millions of individual DNA molecules and (2) evaluation of energies of intermolecular interactions in short DNA duplexes or in other molecules. Finally, we have shown that DNA duplexes dissociation is mediated by mechanical stress and produced by the movement of magnetic nanoparticles in magnetic fields, but not by local overheating. The presented technique opens a new avenue for high-precision manipulation of DNA and generation of biosensors for quantification of energies of intermolecular interaction.

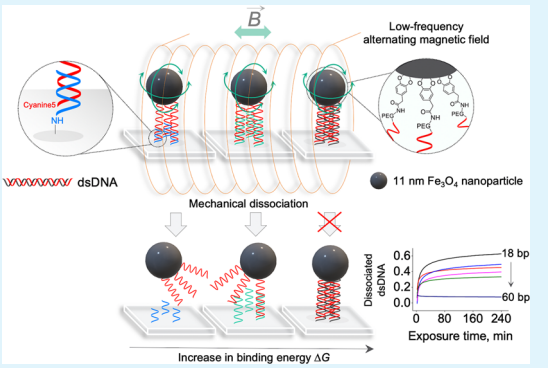

KEYWORDS: *magnetic nanoparticle, DNA, magnetic field, mechanical force, magnetic actuation, remote control, magneto-mechanics*

INTRODUCTION

Recent studies on the remote control of various macromolecules using magnetic nanoparticles (MNPs) exposed to nonheating external magnetic fields resulted in enhanced efficiency of drug delivery,[1] selective magneto-mechanical cell death,[2−5] regulation of autophagy in mouse B-lymphoma cells,[6] remote control of the ion channels of the cell membranes,[7] and the activity of various enzymes.[8] Conjugates based on magnetic particles and DNA have been used as biosensors, for pathogen detection and molecular targeting.[9,10] Also, the remote control of macromolecules in real time using magnetic particles in external magnetic fields is of particular interest in the DNA origami technique for reconfiguring various DNA assemblies, which can be used, e.g., for creating self-assembling and self-destructing drug delivery vessels.[11]

Nowadays, the magnetic tweezers technique is commonly used to manipulate individual molecules.[12] Despite the fact that such a technique is a powerful tool, which has a high spatial resolution and significantly succeeded in stiffness measurements of cell membranes,[13] as well as in quantifying the strength of various ligand-receptor pairs,[14] it cannot be applied in experiments with small single MNPs. When the size of a magnetic nanoprobe is reduced to the nanometer range, a number of problems arise due to the inability to track the position of such a probe using optical microscopy. This makes it impossible to quantify the effect of a small individual MNP on various macromolecules or even cells in magneto-mechanical experiments at a single-molecule level.[15,16]

Lack of unambiguous attempts on accurate measurements of energies/torque/forces transmitted from small individual MNPs to conjugated macromolecules under the influence of external nonheating magnetic fields and also incomplete understanding of the processes taking place lead to drastically contradictions when trying to quantify the observed effects. Often, the assessment of whether we can manipulate macromolecules using small individual MNPs is based on experiments with aggregates of such MNPs, which results in significant deviations in the evaluation of the determined values and requires theoretical models that can distinguish the contribution of a single MNP to the averaged experimental signal.[17,18] As a result, e.g., an attempt to compare the stretching force values that individual MNPs can mediate and transfer to macromolecules under external magnetic field

Received: November 26, 2020
Accepted: March 10, 2021
Published: March 19, 2021

https://doi.org/10.1021/acsami.0c21002
ACS Appl. Mater. Interfaces 2021, 13, 14458−14469

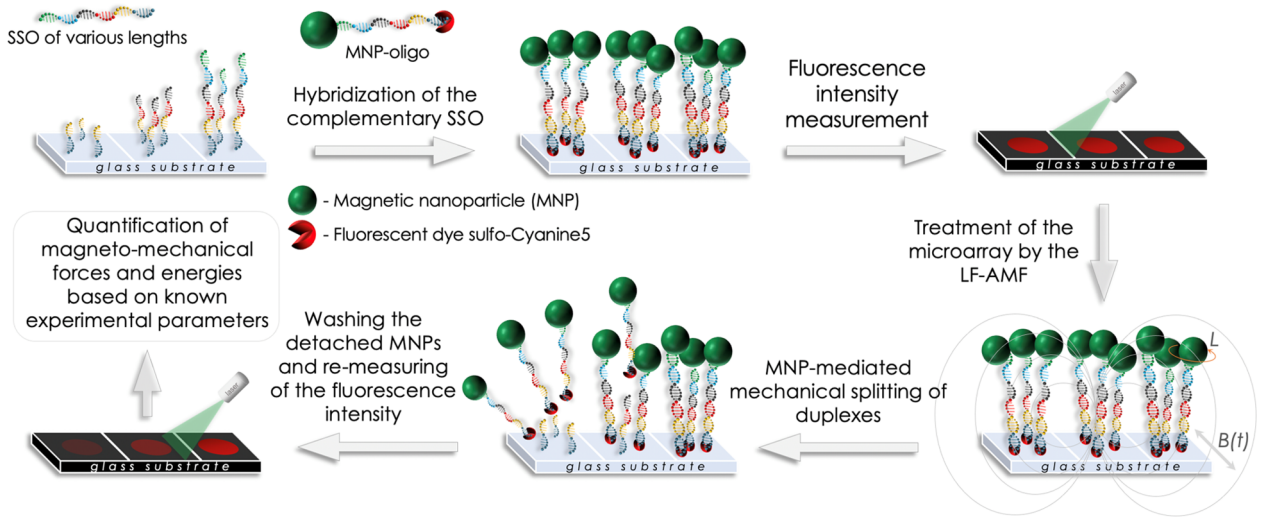

Figure 1. Step-by-step schematic illustration of the experimental strategy.

exposure leads to discrepancies of up to 13 orders of magnitude (from 10^{-20} to 10^{-7} N for MNPs with core radius ≤500 nm).[19−25]

Thus, the question arises: what effect on macromolecules do we actually observe from individual MNPs? This is especially important to consider when external alternating magnetic fields are used for such manipulations. In this case, it is necessary to understand how the field energy is converted into MNPs mechanical motion and transferred to the attached macromolecules. The most direct way to answer this question is performing single-particle studies to avoid secondary effects originating from MNP aggregates. MNP analysis in powders or at a high concentration in solvent can also lead to significant deviations and incorrect interpretation of the obtained results.

In this regard, this work is a proof of principle of the operability of the magneto-mechanical manipulation technique using individual MNPs. In our experiments, we used a series of fluorescently labeled synthetic DNA duplexes with different binding energies between complementary strands conjugated with individual 11 nm MNPs. It is well known that DNA duplexes with a given sequence and length have well-defined thermodynamic dissociation energy. Therefore, they can be used as model molecules to answer the main question of this study.[26,27] The resulting DNA-MNPs conjugates, fixed on a glass substrate, were exposed to a low-frequency alternating magnetic field (LF-AMF), which led to rotational movements of MNPs and caused deformation of the DNA duplexes conjugated to them. When the MNP-mediated magneto-mechanical effect was sufficient to separate DNA strands, this separation led to the dissociation of fluorescently labeled MNPs from the glass surface, which was detected using a confocal scanner.

The developed technique allows simultaneous manipulation of many individual DNA molecules in a single run at a statistically significant level. Moreover, our technique is versatile, so it opens an avenue for evaluation of the efficiency of the magneto-mechanical manipulation of various macromolecules using MNPs of any size, shape, and phase composition. In addition, thanks to the precisely tuned parameters of the magnetic field and the properties of MNPs, one can accurately control the magnitude of the magneto-mechanical effect and, as a consequence, the degree of the influence of MNPs on macromolecules conjugated with them. Finally, using various chemical routes, one can conjugate MNPs with any type of fluorescent dyes and therapeutic agents and also conjugate a determined number of identical molecules with a single MNP, which allows us to study the collective response of such molecules on the external mechanical stress.

RESULTS AND DISCUSSION

Experimental Strategy. To evaluate the possibility of the remote control of various molecules using single MNPs exposed to a nonheating LF-AMF, we developed the experimental technique shown in Figure 1. We designed a series of single-stranded oligonucleotide (SSO) targets of different lengths bearing 3′-amino group for immobilization on a glass support and a complementary SSO-probe 5′-labeled with sulfo-Cyanine5 dye (sCy5) and bearing 3′-amino group for conjugation with MNPs (Table 1, Supporting Information, Section I). SSO-targets were designed with a guanine-cytosine (GC) content of 33−50% and tuned sequences to avoid stable internal structures and self-dimers. The length of SSO was chosen based on the melting temperature predicted by Mfold calculations[28] in the range of 45−71 °C in about 5 K steps. SSO-targets were covalently attached to a glass surface (Figure S1), while SSO-probes were conjugated with MNPs by amide linkage (MNP-oligo) (Figure 2A). Then, MNP-oligo conjugates were hybridized to oligonucleotide microarrays on the glass surface. Finally, the microarrays were exposed to an LF-AMF, resulting in rotational movements of MNPs mediated by a magnetically driven torque. Such a torque was transferred from an MNP to the covalently linked DNA duplexes through the stretching force, which resulted in mechanical deformations and separation of DNA strands followed by washing out released MNP-oligo. Thus, measuring the fluorescence of the microarrays before and after LF-AMF exposure allowed us to evaluate the relationship between the mechanical properties of DNA duplexes and the magneto-mechanical effect implemented by a single MNP in LF-AMF.

Characterization of MNPs and Their Conjugation to SSO-Probes. We synthesized cubic MNP-oligo conjugates with an average magnetic core size of 11 ± 2 nm (Figure

https://doi.org/10.1021/acsami.0c21002
ACS Appl. Mater. Interfaces 2021, 13, 14458−14469

Table 1. SSO Used in This Work

oligonucleotide		sequence 5′ → 3′	GC content (%)	T_m [b] (°C)	ΔG^b (kcal·mol^{-1})
SSO-probe	60 nt[a]	sCy5-TGTATCGGAACATCAATTGTGCATCGCGCCAGCATAATCATGTCATCTGCGAAGTGGACG(T)$_5$-NH$_2$	48		
SSO-targets	18 nt	AATTGATGTTCCGATACA(T)$_{10}$-NH$_2$	33	45.6	19.7
	21 nt	CACAATTGATGTTCCGATACA(T)$_{10}$-NH$_2$	38	50.7	24.6
	25 nt	GATGCACAATTGATGTTCCGATACA(T)$_{10}$-NH$_2$	40	55.8	31.0
	28 nt	CGCGATGCACAATTGATGTTCCGATACA(T)$_{10}$-NH$_2$	46	61.2	38.9
	32 nt	CTGGCGCGATGCACAATTGATGTTCCGATACA(T)$_{10}$-NH$_2$	50	65.0	46.5
	60 nt	CGTCCACTTCGCAGATGACATGATTATGCTGGCGCGATGCACAATTGATGTTCCGATACA(T)$_{10}$-NH$_2$	48	71.1	90.9

[a]nt: nucleotides. [b]Melting temperature of DNA duplexes T_m and Gibbs energy ΔG of DNA dissociation in 100 mM NaCl and 3 mM $MgCl_2$ were predicted using OligoCalc.[55]

2B,C) and two different percentages of loading of SSO-probe per single MNP. Using an ssDNA-binding fluorescent dye assay, which is accurate to tenths of ng ssDNA per μL of solution, we quantified that single MNPs are functionalized by 2 (MNP-oligo-2) or 12 (MNP-oligo-12) chains of SSO-probe (Supporting Information, Section II). The ability to selectively functionalize MNPs using chemical routes allows us to study the magneto-mechanical effects in experiments with both a single DNA duplex and with a group of identical DNA duplexes. DLS analysis after each modification step showed that MNP-oligo do not aggregate in aqueous solutions and are present in them in the form of single cores (Figures 2D, S2−S4, Tables S2−S4). Since any free SSO-probe in the MNP-oligo solution will bind to SSO-targets that will lead to false analysis in further steps, we confirmed that conjugates are stable over time under all experimental conditions. We observed no SSO-probe leakage from MNP-oligo conjugates even after incubation of the solutions of such conjugates in hybridization buffer at 62 °C for 3 h (Figure S7, Supporting Information, Section II).

The XRD analysis showed that produced MNPs crystallized in the magnetite phase (Fe_3O_4, ICDD PDF-2 no. 00-19-0629) (Figure 2E), while the size of a single crystallite is 9.462(6) nm and agrees reasonably well with the data obtained by the TEM analysis. Because the lattice parameter of a bulk magnetite (Fe_3O_4, a = 0.8397 nm) is close to that of a bulk maghemite (γ-Fe_2O_3, 0.8347 nm), we also performed the Mössbauer spectroscopy analysis, which also confirmed the formation of Fe_3O_4 phase (Figure S8a, Table S5). The specific magnetization values of MNPs were recalculated to the pure magnetic phase using thermogravimetric analysis in the temperature range of 30−500 °C and AES analysis (Figure S8c, Supporting Information, Section III).

Figure 3A,B presents the magnetic hysteresis loops at various temperatures for oleic acid-stabilized MNPs (MNPs@OA) and MNP-oligo-12, respectively. Due to the restrictions of the solvents, we compared the specific saturation magnetization M_S at 200 K and found M_S = 101 A·m^2·kg^{-1} for MNPs@OA in chloroform and M_S = 66 A·m^2·kg^{-1} for MNP-oligo-12 in water, which were reached at B = 5 T and B = 2.5 T, respectively. Note that the error bar was estimated to be about 10% of M_S due to the small volume (10 μL) of liquid probes and the low content of MNPs. Considering this, the obtained M_S value matches the range of volumetric values at 5 K (96.4 A·m^2·kg^{-1}) and 300 K (92.0 A·m^2·kg^{-1}).[29] After functionalization of MNPs with SSO-probe, M_S is reduced by 35%, which we ascribe to partial oxidation γ-Fe_2O_3 and the growing error bar at a lower concentration of Fe in the liquid probes. Most important here is that sufficiently high magnetization is reached at small inductions used in LF-AMF treatments. We obtain magnetizations of 45−73%·M_S in 20−100 mT at 200 K and anticipate similar values at 300 K. Figure 3C shows the coercive fields as a function of temperature $T^{2/3}$. In this scaling, the coercive field decreases linearly as indicated by the broken lines. Note that nonzero values at 100 K (about 22 K$^{2/3}$) originate from the largest MNPs. The plot allows determining the effective magnetic anisotropy energy density K_{eff} from a linear fit following Sharrock's approach for single-domain, randomly oriented, noninteracting MNPs and reads.[30,31]

https://doi.org/10.1021/acsami.0c21002
ACS Appl. Mater. Interfaces 2021, 13, 14458−14469

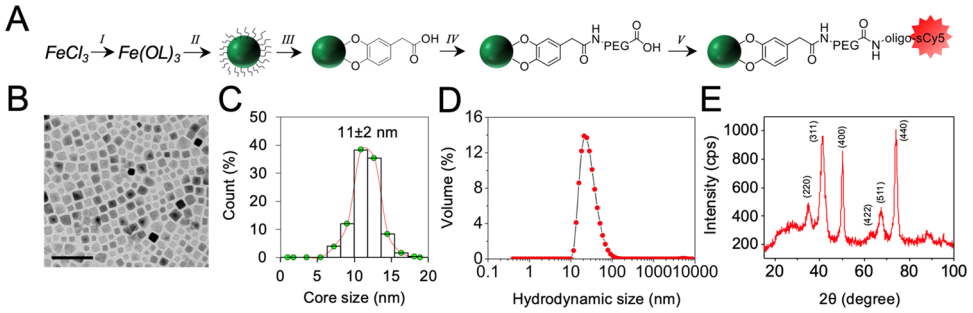

Figure 2. Characterization of functionalized nanoparticles. (A) Step-by-step synthesis scheme of MNP-oligo. (I) Preparation of iron(III) oleate complex from iron(III) chloride. (II) Thermal decomposition of iron(III) oleate resulting in the formation of hydrophobic oleic acid (OA)-stabilized MNPs@OA. (III, IV) Hydrophilization of MNPs using ligand exchange technique. (V) Modification of hydrophilic MNPs with SSO-probe molecules. (B) TEM image of MNP-oligo-12. Scale bar: 50 nm. (C) Histogram of MNP-oligo-12 core size distribution. (D) Hydrodynamic diameter of MNP-oligo-12 in PBS at pH = 7.4. (E) XRD pattern of MNPs@OA with Miller indices of the Bragg peaks in an inverse spinel structure (cps, counts per second).

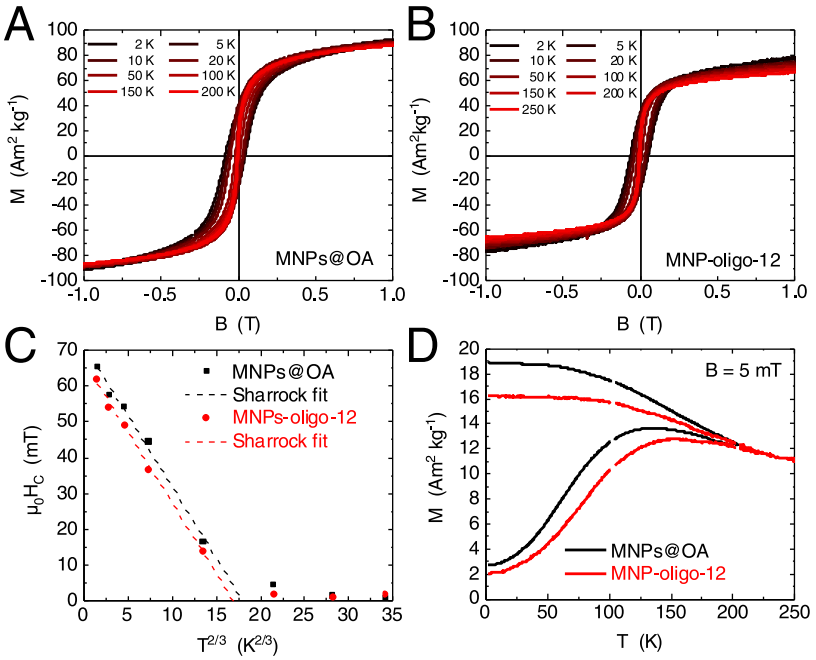

Figure 3. Magnetometry of MNPs before and after functionalization. (A) Hysteresis loops at various temperatures for the pristine MNPs@OA stabilized by oleic acid in chloroform. (B) Hysteresis loops of functionalized MNP-oligo-12 in water. (C) Coercive field as a function of $T^{2/3}$ and the corresponding fit according to the Sharrock model. (D) Zero-field-cooled and field-cooled magnetization as a function of temperature. The magnetization is calculated using the Fe_3O_4 mass and the Fe content determined by thermogravimetric analysis and AES analysis. Before magnetometry, the liquid samples were first frozen in zero field to reduced influence of dipole−dipole interaction. Thus, measurements are restricted to temperatures significantly below the melting point of chloroform (210 K) and water (273 K).

$$\mu_0 H_C(T) = \mu_0 H_C\ (T = 0\ \mathrm{K}) \cdot \left[1 - \left(\frac{T}{T_B}\right)^{2/3}\right]$$

This approach averages over all MNP sizes of a mass distribution. Fitting $\mu_0 H_C(T)$ yields an average blocking temperature T_B, which can be translated into K_{eff} via $21 \cdot k_B T \approx K_{eff} \cdot V_{MNP}$, where k_B is the Boltzmann constant and V_{MNP} is the MNP volume. The pre-factor 21 accounts for an attempt frequency of 10^9 Hz and the time window of 1 s in VSM. We obtained very similar average blocking temperatures of T_B = 72 K for MNPs@OA and T_B = 69 K for MNP-oligo-12. Thus, the magnetic anisotropy of MNPs does not change upon functionalization and transfer to water. Further, K_{eff} is calculated to about 30 kJ·m^{-3} for both samples. This result is enhanced compared to the first-order anisotropy constant of volumetric Fe_3O_4 K_1 = 13 kJ·m^{-3}, but fits well in the size-dependent anisotropy recently published.[29] The ZFC/FC curves in Figure 3D give an irreversibility temperature of about 200 K, which is the blocking temperature T_B of the largest MNPs, while the maximum of the ZFC curves is at 120 and 150 K for the pristine and functionalized MNPs, respectively. Importantly, for all following experiments at ambient temperature, the MNPs are in the superparamagnetic state.

Immobilization of SSO-Targets on the Glass Surface and Hybridization to Complementary SSO-Probes. Of note, the fluorescence patterns of the microarrays after hybridization of SSO-targets with MNP-oligo-2 and MNP-oligo-12 differed fundamentally (Figures S9 and S10A). We assume that a decrease of the total number of SSO-probe per single MNP resulted in a decrease of the total binding energy

https://doi.org/10.1021/acsami.0c21002
ACS Appl. Mater. Interfaces 2021, 13, 14458−14469

of oligonucleotide complementary strands after their hybridization. As a result, after hybridization of SSO-targets with MNP-oligo-2, the clear fluorescent pattern was observed only for 60 bp duplex (Figure S9). Taking into account that MNPs undergo thermal vibrations ($k_BT \sim 4 \times 10^{-21}$ J at T = 300 K) even in the absence of external magnetic fields, they induce an undirected mechanical vibration. As a result, thermal fluctuations of MNPs can cause the partial dissociation of complementary base pairs.[32]

To prove that the binding of MNP-oligo to the microarray surface is specific to the hybridization of MNP-oligo with complementary SSO-targets and is not a result of nonspecific adsorption, we synthesized sCy5-labeled nanoparticles MNPs@sCy5 without SSO-probe and added their solution to the microarray covered with SSO-targets. Scanning of the processed microarray showed no differences of the fluorescence intensity between spots and background fluorescence (Figure S11), which confirms the specific binding of MNP-oligo to the microarray by duplex formation. We also showed that repeated scanning of the microarrays does not fade the sCy5 signal under the laser exposure (Figure S12).

To estimate the number of successful hybridizations per MNP in each case, we additionally performed experiments with SYBR green I dye, which is highly specific to DNA duplexes. For this, during the hybridization, we also used pure SSO-probe solutions with the same SSO-probe concentration as in its conjugates with MNPs (MNP-oligo-2 or MNP-oligo-12). It is noteworthy that the fluorescence intensity of SYBR Green I was higher when using pure SSO-probes during hybridization (Figure S13A,B). Comparison of the SYBR Green I fluorescence intensity normalized to the sCy5 fluorescence intensity results in similar patterns for both MNP-oligo-2 and MNP-oligo-12 conjugates (Figure S13C). This result indicates that, in the case of MNP-oligo conjugates, only half of SSO-probes fixed on the MNP surface can form DNA duplexes with SSO-targets fixed on a glass substrate.

Theoretical Substantiation of the Magneto-Mechanical Effect Mediated by Individual MNP in LF-AMF. First, we want to emphasize that the magnetic field gradient in the working area (area of the microarray location) did not exceed 0.1% ($\nabla B \sim 0.1$ mT·m^{-1} at B = 100 mT) in our experiments (Figure S14). As the magnetic field gradient was so small, we can safely neglect a linear movement of the MNP in the quantification.[33] As mentioned above, the MNPs are superparamagnetic, so the magnetic moments m of MNPs are oriented randomly in zero field at 25 °C. In inductions of B = 20−100 mT, however, the magnetic landscape is modified and strongly favors the alignment of m parallel to B and fluctuations are at least partially suppressed. We have chosen this range of B since many mechano-chemical processes in living organisms were shown to occur at such magnetic field amplitudes.[34]

There are two well-known relaxation channels of MNPs in liquid media in an external LF-AMF: Néel and Brown relaxations.[34,35] These mechanisms coexist and depend on the MNP size, magnetic properties, and its environment. In the case of Néel relaxation, the MNP is motionless, while its magnetic moment rotates relative to the crystal structure; however, in the case of Brownian relaxation, the MNP magnetic moment aligns to the applied magnetic field direction via the mechanical rotation of MNPs.[36,37] It is very important that for low frequencies of <1 kHz (nonheating regime), the MNP magnetization response dominantly occurs by the Brownian relaxation because the contribution of the Néel relaxation to the magnetization dynamics in this case is minimal.[38] In addition, considering the very high density of MNP-oligo on the microarray surface after hybridization of SSO complementary strands, one can assume that the distance between the individual MNPs is minimal, which can result in large dipole−dipole interaction and, therefore, declining magnetization in the Néel regime.[38]

Based on previous theoretical works,[5,34,39] we can propose that there are only several routes of Brownian MNP oscillation in LF-AMF that help us to understand the magnetically driven processes occurring with DNA duplexes conjugated to individual MNPs. At the initial moments (B = 0), the direction of the MNP magnetic moment vector m is generally unknown. Thus, by the time the LF-AMF is switched on, there are several possible orientations of the vector m relative to the field induction vector B. In the first route (Figure S15B(1)), vector m is already parallel to the vector B, and, as a consequence, MNP will not have any effect on the DNA duplex, freely turning around a single covalent chemical bond. In the second route, the vector m is not parallel to the vector B and tends to align in its direction through the rotation of MNP, while the angle between such vectors is in the range of $0° < \alpha < 180°$. Let us consider the case when $\alpha = 90°$ (Figure S15B(2,3)) and, therefore, MNP acts as a "lever", leading to the stretching of the DNA duplex. Previously, it was shown that to cleave the DNA hairpins in such geometry, the values of the stretching force should reach 20−50 pN.[40,41] The only way in which the vector m can align in the direction of the vector B is the tilt of the DNA duplex relative to the substrate surface. However, taking into account the size of the MNP, as well as the fact that under experimental conditions the MNP is surrounded by other MNPs, the vector m does not align parallel to vector B. As a result, the MNP will tend to rotate, thereby mediating the stretching force transmitted to the attached DNA duplex. In this case, worm-like chains[42] of DNA duplexes are fully extended by very small forces of the order of 0.5 pN, which are enough to melt the DNA duplex,[16,39] while the critical torque value exerted on the MNP is about 9 pN·nm.[16,43−45] Moreover, it should be noted that the interactions of individual base pairs are very weak (only a few k_BT), and MNP thermal fluctuations lead to opening the DNA duplex from its end.[46] For instance, the force only of 0.039 pN is required to perform mechanical separation of A−T base pair.[47] The shorter the DNA duplex, the more likely every base pair will detach, and two strands will separate even at very low forces.

Since in our case the angle α is generally unknown, the magnetic torque reads as

$$\vec{L} = \vec{m} \times \vec{B}$$

The maximum torque can be reached for $\alpha = 90°$ for the maximum induction B = 100 mT and the average magnetic moment of MNPs of 1.18×10^{-19} A·m^2 (Supporting Information, Section V)

$$|\vec{L}| = |\vec{m}||\vec{B}| \sin\alpha = 1.18 \times 10^{-20}\ \text{N·m} = 11.8\ \text{pN·nm}$$

Of note, the obtained torque value exerted on the 11 nm MNP is in good agreement with previous theoretical calculations.[34,39] Hence, the magneto-mechanical stretching

https://doi.org/10.1021/acsami.0c21002
ACS Appl. Mater. Interfaces 2021, 13, 14458−14469

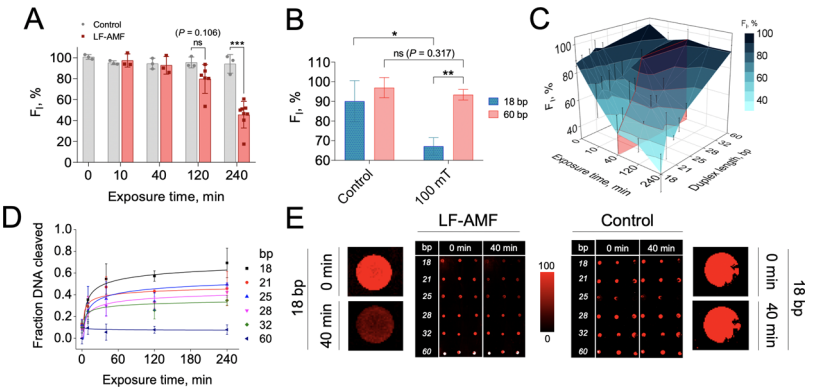

Figure 4. Influence of the LF-AMF (f = 180 Hz, B = 100 mT) on the DNA duplex dissociation. (A) Dependence of the sCy5 fluorescence intensity on the LF-AMF exposure time for 60 bp duplex formed by MNP-oligo-2. (B) Normalized fluorescence intensity after 10 min treatment of 18 and 60 bp duplexes (MNP-oligo-12) by LF-AMF (n = 3). (C) 3D plot of LF-AMF influence on the normalized fluorescence as a function of duplex length and magnetic field exposure time for duplexes formed by MNP-oligo-12 (n = 6). (D) Dependence of the fraction of dissociated DNA duplexes on the magnetic field exposure time for DNA duplexes formed by MNP-oligo-12. Data are mean ± SD. Statistical significance was calculated by one-way ANOVA test (n = 3, *P < 0.05, **P < 0.01, ***P < 0.001, ns: nonsignificant). (E) Representative images of the control microarray and microarray with DNA duplexes formed by MNP-oligo-12 before and after 40 min treatment with LF-AMF.

force, which can be exerted on the DNA duplex attached to MNP with magnetic core radius R_{MNP} = 5.5 ± 1.0 nm is

$$F_M = \frac{L}{R_{MNP}} = 2.1 \pm 0.4 \text{ pN}$$

Thus, based on the described theoretical models and calculations, we expect that the value of the calculated stretching force mediated by 11 nm MNP will be enough for manipulation and significant dissociation of DNA duplexes.

Experimental Study of the DNA Duplex Dissociation. After careful characterization of MNP properties and theoretical estimations, the corresponding practical experiments were carried out. After hybridization procedure, all microarrays with attached duplexes were put into PBS solution (pH = 7.4) and treated by LF-AMF at various modes, while the maximum exposure duration was 240 min. To avoid the temperature-related effects, we used nonheating ultra LF-AMF, and after each treatment of microarrays with LF-AMF, we additionally monitored their surface temperature using an infrared camera. Moreover, we exclude the local overheating on MNP surface relatively to the surrounding medium, which is negligible and is not more than 10^{-10} K under our conditions (Supporting Information, Section VI).

Initially, we examined the dissociation of 60 bp DNA duplex formed using MNP-oligo-2. We treated the microarrays at the largest amplitude value B = 100 mT for various times. As a result, 240 min of field exposure led to ∼55% detachment of the fluorescent MNP-oligo-2 conjugate (Figures 4A and S9). In summary, considering the estimation of the number of successful hybridizations per MNP (Figure S13), the results suggest that if two SSO-probes are conjugated to single MNPs, only one can form a duplex with the SSO-target on the 2D glass surface. The collinear arrangement of SSO-probe strands fixed on the MNP surface favors minimization of the intermolecular interaction and total system energy[48] and, therefore, results in the formation of a single duplex on the 2D glass surface. Moreover, the collinear arrangement of two SSO-probes on the surface of 20 nm gold particles was also previously proved by TEM analysis after conjugation of such particles with 5 nm gold particles bearing one complementary SSO-target.[49] Thus, it can be assumed that in this case, MNP transfers to a single 60 bp DNA duplex a sufficient amount of energy for its dissociation. Moreover, based on the described magneto-mechanical models, we can also assume that the theoretically predicted value of the stretching force $F_M \approx 2$ pN mediated by MNP is in good agreement with our experimental results.

Then, we examined the collective dissociation of the same DNA duplexes and processed microarrays containing duplexes formed using MNP-oligo-12. The increase in the number of SSO-probes per single MNP (from 2 to 12) leads to a strong increase in total binding energy of such MNP with substrate after hybridization, and as a result, we conclude that larger times, energies, and forces are required to dissociate all DNA duplexes. First, we processed the microarrays for 10 min at magnetic induction B in the range of 20−100 mT. As in the previous case, the most notable effect of LF-AMF on the separation of DNA strands was observed at the largest amplitude value B = 100 mT and only for 18−28 bp duplexes, while no changes of the fluorescence were detected for the 60 bp duplex (Figures 4B and S16).

One can explain the observed effects by simple local overheating near the surface of MNP, leading to melting of DNA duplex. However, our findings suggest the magneto-mechanical nature of the observed effect. Indeed, if the local heating takes place, we will observe the same dissociation curves for MNP-oligo-2 and MNP-oligo-12 in the case of 60 bp duplexes because heating is produced by MNP, which is same in both cases, thus leading to the same heating rates and melting of all surrounding DNA duplexes, regardless of their amount per single MNP. Obviously, differences in results for duplex dissociation formed by MNP-oligo-2 and MNP-oligo-12 show that this is not the case. In addition, it was previously experimentally shown that even in the hyperthermia regime, when the field frequency f is several hundred kilohertz, local overheating on the surface of a 15 nm iron oxide MNP is negligible even at a distance of several nanometers from their surface, which is several times less than the thickness of the organic shell in our case.[50]

Because the most pronounced effect was observed at B = 100 mT, we used this amplitude to determine the influence of the LF-AMF exposure time on the collective duplex dissociation. We investigated four exposure durations (10,

https://doi.org/10.1021/acsami.0c21002
ACS Appl. Mater. Interfaces 2021, 13, 14458−14469

40, 120, and 240 min) and obtained the corresponding microarray images as a result (Figure S10A). Of note, the magneto-mechanical effect becomes more apparent for longer LF-AMF exposures. After 40 min of LF-AMF exposure, an asymptotical dependence of the degree of the duplex strand separation on the duplex length is clearly observed (Figure S10B). Furthermore, τ = 120 and 240 min of LF-AMF exposure resulted in partial dissociation of 32 bp duplex (26 ± 8 and 35 ± 5%, respectively), and the portion of dissociated 18−28 bp duplexes increased in all cases. The three-dimensional plot clearly shows that the portion of dissociated duplexes increases with the exposure time and upon reduced duplex lengths (Figure 4C). It is interesting that the obtained kinetic curves indicate that in each case, even after 240 min of LF-AMF exposure, there is a fraction of undissociated DNA duplexes, i.e., the degree of dissociation cannot reach 100% (Figure 4D). This fact is in good agreement with our theoretical predictions regarding the routes of Brownian MNP oscillation in LF-AMF. The dissociation degree equal to 100% cannot be achieved, since at the initial moments, there is always a certain fraction of MNPs whose magnetic moment is already oriented parallel to the vector B and due to free rotation of single bonds in DNA, they have no effect on the DNA duplexes conjugated with them during the treatment by LF-AMF. Moreover, the longer the DNA duplex, the more flexible it is and the greater the possibilities that it is able to resist and suppress MNP oscillations.

Unlike the magnetic tweezer technique, where the applied stretching force mediated by magnetic microbeads is stable throughout the experiment (if the distance between the magnet and such microbeads remains constant), under our conditions, this force changes its value every time with a change in the direction of vector B, while the value of this force depends on the initial direction of the MNP magnetic moment relative to the vector B. Thus, DNA duplexes are not subjected to a constant mechanical stress, which allows dissociated complementary base pairs to rehybridize. As mentioned above, under the LF-AMF exposure, MNPs undergo frequent rotational movements, which causes constant twitching of the DNA duplex. At the same time, to understand the processes occurring in this case, the mechanical response of DNA duplexes can be compared with Velcro. At a high constant stretching force or at a high force-loading rate, the Velcro strips can be easily separated in times of the order of milliseconds, as in the magnetic tweezer technique. However, at low values of the force, the process of strand separation will have a pronounced statistical character. With an increase in the duration of the effect of an external force on the DNA duplex, the number of dissociated complementary bases will increase, and at one of the moments when their number is equal to or exceeds the number of hybridized (rehybridized) bases, DNA strand separation will occur. Our assumption is also well supported by previous study, where the authors described the same asymptotic dissociation kinetics (Figure 4D) and similar order of dissociation times in experiments on long dsDNA using highly parallel magnetic tweezers.[51] Moreover, to remove MNP-oligo-12 from the microarray surface, all complementary base pairs should be disconnected in each duplex. However, in the case of more than one duplex formed per single MNP, this process is complex and cannot be described by a linear function. Taking into account the differences in the results after hybridization of SSO and LF-AMF processing, we suppose that several SSO-probes (in the case of MNP-oligo-12) can form duplexes with a complementary SSO-target on a glass surface. This is also confirmed by the fact that, in the case of MNP-oligo-12, the 60 bp duplexes remained intact even after 240 min of exposure; hence, an individual MNP cannot provide sufficient energy transfer from the magnetic field to several 60 bp DNA duplexes for their dissociation. Of note, at the same time, the groups of identical duplexes consisting of up to 32 bp were dissociated in this LF-AMF mode (Figure S10B). Thus, taking into account the fact that we observed the dissociation of a group of 32 bp duplexes formed by MNP-oligo-12 at similar times of dissociation of a single 60 bp duplex formed by MNP-oligo-2, we can assume that the energy transferred from individual MNP with a size of 11 nm in an LF-AMF with f = 180 Hz and B = 100 mT to the attached DNA duplexes is not less than ∼90 kcal·mol^{-1} (Table 1). Using a such technique, one can obtain the experimental values of the energies transferred by individual MNPs of any sizes, shapes, and phase compositions in LF-AMF with known parameters. These findings can be used in future works to construct a calibration curve, which will be useful for a quantitative assessment of unknown energies of various intermolecular interactions.

CONCLUSIONS

In this work, we demonstrated a proof of principle of using individual 11 nm MNPs as a tool for remote-controlled mechanical detachment of short DNA duplexes (18−60 bp). We showed that the mechanical vibrations mediated by individual MNP under LF-AMF influence are transmitted to DNA duplexes in the form of stretching force with the maximum value of about 2 pN, which is enough to dissociate dsDNA with binding energy 90 kcal·mol^{-1}. Additionally, we demonstrated that the effect of duplex dissociation is time- and sequence-dependent, can be adjusted by changing the magnetic field parameters, and is not related to the local heating of a nanoparticle. Undoubtedly, for the most complete understanding of magneto-mechanical effects in experiments using MNPs, further studies of mechanisms as a function of MNP size, shape, composition, and field parameters are necessary. We are confident that the results presented in this work will be applied in upcoming studies on remote control of various molecules and also individual cells by magnetically driven forces.

MATERIALS AND METHODS

Design and Synthesis of ss-Oligonucleotides (SSO). SSO-targets were designed to avoid stable internal structures and self-dimers with a guanine-cytosine (GC) content of 30−50%. SSO were assembled in a Mermaid 6/12 DNA synthesizer by the phosphoramidite method according to the manufacturer's recommendations. Protected 2′-deoxyribonucleoside 3′-phosphoramidites, *N*-(6-(*O*-dimethoxytrityl)-hexyl)-(2-carboxamide)phthalimidyl-lcaa-CPG 500 Å, and *S*-ethylthio-1*H*-tetrazole were purchased from ChemGenes; 5′-alkyne phosphoramidite and sCy5 azide were obtained from Lumiprobe LLC. Oligonucleotides were cleaved from the support and deprotected using concentrated aqueous ammonia at 55 °C overnight. SSO were double-purified by denaturing PAGE followed by RP-HPLC. 5′-sCy5 labeling was performed as described earlier.[52] Oligonucleotide purity was confirmed by ESI-MS using Bruker Maxis Compact q-TOF.

Synthesis of Oleic Acid-Stabilized MNPs (MNPs@OA). Oleic acid-stabilized MNPs were synthesized by thermal decomposition of iron oleate(III) in the presence of oleic acid as described earlier.[53]

https://doi.org/10.1021/acsami.0c21002
ACS Appl. Mater. Interfaces 2021, 13, 14458−14469

Briefly, for the preparation of an iron oleate complex, 6 mmol of sodium oleate (95%, ABCR GmbH & Co. KG) was dissolved in a mixture of distilled water (40 mL), 96% ethanol (40 mL), and *n*-hexane (80 mL). Then, 2 mmol of iron(III) chloride (97%, reagent grade) was added to this solution. The resulting mixture was heated to reflux under vigorous stirring and kept at this temperature for 4 h. After cooling the mixture to room temperature, the upper brown-black layer was separated, washed three times with distilled water and ethanol (v/v = 1:1), and dried under vacuum. Thus, a viscous iron oleate complex was obtained. To synthesize iron oxide nanoparticles, a mixture of 4 mmol of iron oleate complex, 1.3 mmol of sodium oleate, and 1.3 mmol of oleic acid (tested according to Ph. Eur.) was dissolved in 33 mL of 1-octadecene. The mixture was heated to 140 °C under argon flow and vigorous stirring (4000 rpm) and kept at this temperature for 1 h to remove water traces. Then, the mixture was heated at a rate of 4 °C·min^{-1} to a reflux temperature and maintained under an argon atmosphere for 30 min. The resulting solution was cooled down to room temperature, and 2-propanol was added to precipitate MNPs@OA. Finally, MNPs@OA were separated by centrifugation (14 000 rpm) and redispersed in *n*-hexane or chloroform.

Surface Modification of MNPs@OA with DOPAC. DOPAC-stabilized MNPs were synthesized according to a slightly modified previously described procedure.[54] NaOH (24 mg, 97%, Sigma-Aldrich) was dissolved in 10 mL of dried CH_3OH (99.8%, Sigma-Aldrich), followed by the addition of 51 mg of 3,4-dihydroxyphenylacetic acid (DOPAC, 98%, Sigma-Aldrich). To modify the surface of MNPs with DOPAC molecules, 10 mL of MNPs@OA in hexane ([Fe] = 1 mg·mL^{-1}) was added to the prepared mixture. The obtained mixture was incubated for 12 h at 50 °C using a water bath under vigorous magnetic stirring. After cooling the mixture to room temperature, the modified nanoparticles (MNPs@DOPAC) were separated from the supernatant by centrifugation for 20 min at 6000 rpm, rinsed with 10 mL of dried CH_3OH, and redispersed in 10 mL of pure deionized water (DI H_2O). To remove unreacted reagents and trace amounts of CH_3OH, the MNPs@DOPAC water solution was washed three times with pure DI H_2O using centrifugal filters (Millipore Amicon Ultra-4, MWCO 30 kDa). In addition, MNPs@DOPAC was separated from any aggregates by passing through 0.45 and 0.22 μm syringe filters Millex-HV, successively.

Conjugation of MNPs@DOPAC with NH_2-PEG-COOH. The conjugation of MNPs@DOPAC with NH_2-PEG-COOH was carried out using *N*-hydroxysuccinimide (NHS, 98%, Sigma-Aldrich)/1-ethyl-3-(3-dimethylaminopropyl)carbodiimide (EDC, ≥98%, Sigma-Aldrich) chemistry. To activate the carboxyl groups of DOPAC molecules, 1 mL of MNPs@DOPAC ([Fe] = 1 mg·mL^{-1}) was mixed with 14 μL of EDC water solution (10 mg·mL^{-1}) and 8 μL of NHS water solution (10 mg·mL^{-1}), followed by gentle stirring for 20 min by a shaker. After this, MNPs@DOPAC with activated carboxyl groups was passed through a PD-10 desalting column to remove free EDC and NHS. The purified nanoparticle solution was mixed with 100 μL of poly(ethylene glycol) 2-aminoethyl ether acetic acid (NH_2-PEG-COOH, M_n ∼ 1100 g·mol^{-1}, Sigma-Aldrich) water solution (100 mg·mL^{-1}) and stirred overnight at room temperature. Modified nanoparticles (MNPs@DOPAC@PEG) were purified from unreacted molecules by 48 h dialysis (50 kDa dialysis tube), followed by filtration using 0.45 and 0.22 μm syringe filters Millex-HV, successively.

Conjugation of MNPs@DOPAC@PEG with SSO-Probe (MNP-Oligo). EDC water solution (14 μL, 10 mg·mL^{-1}) and NHS water solution (8 μL, 10 mg·mL^{-1}) were added to 1 mL of MNPs@DOPAC@PEG water solution ([Fe] = 50 μg·mL^{-1}) to activate terminal carboxylic groups, and the resulting mixture was stirred for 20 min at room temperature. The excess of EDC and NHS was removed using a PD-10 column. Activated nanoparticles were mixed with 5 μL of freshly prepared 50 or 224 μM aqueous solution of SSO-probe to produce 2 or 12 SSO-probe molecules per single MNP, respectively, and the obtained mixture was stirred in the dark overnight at room temperature. Modified nanoparticles were purified from possible unbound oligonucleotide molecules using the PD-10 column and 48 h dialysis (50 kDa dialysis tube). Moreover, the possible nanoparticle aggregates were removed by filtration using 0.45 and 0.22 μm syringe filters Millex-HV, successively. As a result, the MNP-oligo with different loadings of SSO-probe per single MNP was produced.

Conjugation of MNPs@DOPAC@PEG with sCy5-NH_2 (MNPs@sCy5). EDC water solution (14 μL, 10 mg·mL^{-1}) and NHS water solution (8 μL, 10 mg·mL^{-1}) were added to 1 mL of MNPs@DOPAC@PEG water solution ([Fe] = 50 μg·mL^{-1}) to activate terminal carboxylic groups, and the resulting mixture was stirred for 20 min at room temperature. The excess of EDC and NHS was removed by a PD-10 column. Then, 10 μL of dimethyl sulfoxide (≥99%, Sigma-Aldrich) solution of sulfo-Cyanine5 amine (95%, Lumiprobe) with a concentration 110 μM was added to activated nanoparticles and the resulting mixture was stirred at room temperature overnight. The purification of nanoparticles from possible unbound dye molecules was performed as in the case of conjugation of MNPs@DOPAC@PEG with SSO-probe.

Atomic Emission Spectroscopy (AES). Quantification of the iron concentration was carried out by atomic emission spectroscopy (Agilent 4200 MP-AES) using the calibration curve for the standard samples in the concentration range of 0.1−2 μg·mL^{-1}. Each MNP sample (10 μL) was dissolved in 90 μL of 37% hydrochloric acid during 2 h and diluted 10^4 times with distilled water before measurements.

Absorbance and Fluorescence Measurements. The absorbance spectra were recorded in the 400−800 nm wavelength range using a Thermo Scientific Multiskan GO spectrometer. Fluorescence intensity measurements were performed on a PerkinElmer EnSpire 2300 Multimode Plate fluorimeter. In all experiments, 100 μL of sample solution was placed in a 96-well plate, followed by appropriate measurements, which were made in triplicates.

Transmission Electron Microscopy. A suspension of nanoparticles in water (10 μL with [Fe] = 0.1 mg·mL^{-1}) was dropped onto the surface of a Formvar-coated copper grid (300 mesh), and the solvent was subsequently evaporated. TEM analysis was performed on a JEOL JEM-1400 microscope (120 kV). The analysis of MNP core size distribution was performed using ImageJ software for 1000 individual MNPs.

X-ray Diffraction. XRD pattern of dried MNP powder was obtained at room temperature using an X-ray power diffractometer DRON-4 with Co Kα radiation. The data were collected from 2θ = 20−100° at a scan rate of 0.1° per step and 3 s per point. A qualitative phase analysis was performed by comparison of obtained spectra with PHAN database.

Mössbauer Spectroscopy. ^{57}Fe Mössbauer spectra were measured at different temperatures with an electro-dynamical spectrometer CMS-1104Em, working in the constant acceleration mode. ^{57}Co in a rhodium matrix was used as a source of the resonant γ-irradiation. Isomer shifts were determined in relation to α-Fe.

Magnetometry. Hysteresis loops, zero-field-cooling (ZFC) and field-cooling (FC) measurements, were performed in a Quantum Design PPMS DynaCool system equipped with the vibrating sample magnetometry (VSM) option. For this, 10 μL of liquid samples was put into synthetic capsules and frozen in zero field below the melting point of chloroform (210 K) and water (273 K). The concentrations of Fe were 4.0 and 0.3 mg·mL^{-1} for MNPs@OA and MNP-oligo-12, respectively. The magnetization was calculated from the Fe concentration assuming that Fe_3O_4 MNPs have formed.

Thermogravimetric Analysis. The thermogravimetric curve was plotted on a synchronous thermogravimetric analyzer Netzsch STA 449 F3. A nanoparticle powder was heated in corundum crucibles under an argon flow in the temperature range of 30−700 °C with a heating rate of 10 °C·min^{-1}.

Fourier Transform Infrared (FTIR) Spectroscopy. FTIR spectra of samples were registered on a Nicolet 380 instrument (Thermo Scientific) in the wavenumber range of 400−4000 cm^{-1} using the KBr pellet method.

Dynamic Light Scattering (DLS) Analysis and ζ-Potential Measurements for MNPs and Their Conjugates. DLS analysis

https://doi.org/10.1021/acsami.0c21002
ACS Appl. Mater. Interfaces 2021, 13, 14458−14469

and ζ-potential measurements were performed on a Zetasizer Nano ZS device. The iron concentration in each sample was 0.2 mg·mL^{-1}.

Nanoparticle Stability Assay. MNP-oligo solution (1 mL) in different buffers (Table S1) was placed in sealed disposable cuvettes (1 cm × 1 cm) for DLS measurements and incubated for 10, 20, 30, 40, 50, 60, 90, and 180 min in each buffer. After each checkpoint, the hydrodynamic size of MNP-oligo solution was measured by DLS. Experiments were performed in triplicate. The iron concentration was 0.2 mg·mL^{-1} in each sample.

Quantification of SSO-Probe. QuantiFluor ssDNA kit (Promega) and the standard protocol for quantification of ssDNA in multiwell plates were used for the determination of SSO concentration. QuantiFluor ssDNA dye selectively binds ssDNA or SSO molecules and detects even low concentrations (0.2−400 ng·μL^{-1} per 1 μL of the solution) of such molecules in probes. Fluorescence intensity measurements (492 nm_{Ex}/528 nm_{Em}) of QuantiFluor ssDNA Dye after binding with SSO molecules were performed on a PerkinElmer EnSpire 2300 Multimode Plate fluorimeter.

Immobilization of SSO-Targets on the Glass Surface. SuperEpoxy 2 microarray substrates (Arrayit) were used to firmly fix the SSO-targets with different lengths via amino group at the 3′-end. The immobilization procedure was carried out based on the Arrayit protocol. Briefly, 1 μL of 50 μM SSO (18, 21, 25, 28, 32, and 60 nt) aqueous solutions was dripped onto an epoxy-activated microarray substrate, followed by incubation of the microarray overnight to evaporate water. Then, the free epoxy groups were blocked for 1 h using BlockIT blocking buffer (Arrayit) for ultralow background fluorescence. Finally, the microarray was washed with 1× buffer A (2 min) and 1× buffer B (2 min) supplied by Arrayit and dried (2 s) using a microarray centrifuge supplied by Arrayit. The surface density of SSO-targets after immobilization is provided by ArrayIT and is approximately 10^{12} ssDNA/mm^2.

Hybridization Protocol. Hybridization of the complementary SSO was performed based on the Arrayit protocol. Briefly, 40 μL of 1.25× hybridization buffer (Arrayit) was heated to 40 °C and then mixed with 10 μL of MNP-oligo water solution ($[Fe_3O_4]$ = 0.15 mg·mL^{-1}). The resulting solution was immediately dispensed over the surface of the coverslip, which was then gently put onto the printed microarray placed in an Arrayit hybridization cassette. The cassette was hermetically sealed and placed in a thermostat for 3 h at 62 °C. Then, the coverslip was removed and the microarray containing the formed duplexes was cooled to room temperature and washed with 1× buffer A (5 min), 1× buffer B (5 min), and finally 1× buffer C (1 min) supplied by Arrayit. Residual moisture from the microarray surface was removed within 2 s using a microarray centrifuge supplied by Arrayit.

Estimation of the Number of Successful Hybridizations Per MNP Using SYBR Green I Assay. SYBR Green I (Invitrogen) solution (70 μL, 2.5×) in 1× TE buffer (10 mM Tris, 1 mM EDTA) was dispensed over the surface of the coverslip, which was then put onto the surface of the glass substrates with immobilized 60 bp DNA duplexes. After incubation for 1 h at room temperature, the coverslip was removed and the microarrays were washed with 1× buffer A (10 min), buffer B (10 min), and finally buffer C (10 min) supplied by Arrayit. Residual moisture was removed by centrifugation using a microarray centrifuge supplied by Arrayit.

Dissociation of Oligonucleotide Duplexes in LF-AMF. The glass substrates with oligonucleotide duplexes were placed in a glass tray containing 10 mL of 1× PBS solution. This tray was fixed in a special holder, which was then placed in a low-frequency field generator TOR03/15 electromagnet (Nanomaterials, Tambov, Russia). The processing of the microarrays was carried out in various magnetic field modes, varying the amplitude in the range of 20−100 mT and the exposure time from 0 to 240 min. After the processing, the microarrays were washed with 1× buffer A (5 min), 1× buffer B (5 min), and finally 1× buffer C (1 min) supplied by Arrayit. Residual moisture from the microarray surface was removed within 2 s using a microarray centrifuge supplied by Arrayit, before the microarrays were scanned. The control microarrays were incubated in 1× PBS without LF-AMF treatment for the same time, after which they underwent a similar washing procedure. The temperature control during the microarray processing by the LF-AMF was carried out using a Seek Thermal CompactXR imager. In all experiments, the surface temperature of the microarrays did not exceed 25 °C.

Analysis of Fluorescence on the Glass Surface to Quantify Oligonucleotide Duplexes. Microarray scanning was performed on InnoScan 900 (Arrayit) at a wavelength of 635 nm, detection gain of 90%, and pixel size of 10 μm. The fluorescence intensity of each type of duplexes was calculated over the entire fluorescent spot area using ImageJ software. The change in the fluorescence intensity was quantitatively determined as $Q\% = 100\%\cdot(I_1 - I_2)/I_1$, where I_1 and I_2 are the fluorescence intensities of the spots before and after processing the microarray, respectively.

■ ASSOCIATED CONTENT

Supporting Information

The Supporting Information is available free of charge at https://pubs.acs.org/doi/10.1021/acsami.0c21002.

Schematic representation of epoxy-activated microarray binding with SSO-targets (Figure S1); (I) Fabrication of MNP-oligo; main components of various salt buffers used in the work (Table S1); hydrodynamic curves of MNPs and their conjugates (Figure S2); main hydrodynamic parameters and ζ-potential of MNPs and their conjugates (Table S2); hydrodynamic curves of MNPs@DOPAC@PEG in various salt buffers (Figure S3); main hydrodynamic parameters and ζ-potential of MNPs@DOPAC@PEG (Table S3); main hydrodynamic parameters and ζ-potential of MNP-oligo-12 (Table S4); MNP-oligo-12 stability assay based on hydrodynamic size measuring for 180 min by DLS in various salt buffers (Figure S4); (II) Quantifying the number of SSO-probe molecules fixed on a single MNP; dependence of the QuantiFluor ssDNA dye fluorescence intensity on the SSO-probe concentration (Figure S5); dependence of the MNPs@DOPAC@PEG solution absorbance on its concentration (Figure S6); stability assay of MNP-oligo (Figure S7); (III) Physical characterization of MNPs and their conjugates; characterization of MNPs and their conjugates (Figure S8); calculated Mössbauer spectral parameters (Table S5); (IV) Immobilization of SSO-targets on the glass surface and hybridization to complementary SSO-probes; representative images of the microarrays formed using MNP-oligo-2 before and after treatment by the LF-AMF (f = 180 Hz, B = 100 mT) (Figure S9); influence of the LF-AMF (f = 180 Hz, B = 100 mT) on the cleavage of DNA duplexes in time for MNP-oligo-12 (Figure S10); representative images of the microarray before and after hybridization procedure using MNPs@sCy5 solution containing 0.25 μM sCy5 (Figure S11); representative images of the microarray after three consecutive scans (A) and corresponding histogram of the sCy5 fluorescence intensity after each scan (B) (Figure S12); representative fluorescent images of 60 nt microarrays after hybridization with pure SSO-probe or MNP-oligo and after staining with SYBR Green I. The concentration of pure SSO-probe and MNP-oligo during hybridization was normalized to the SSO-probe content. Histogram of the normalized 532/635 nm fluorescence intensity (Figure S13); (V) Theoretical substantiation of the magneto-mechanical

https://doi.org/10.1021/acsami.0c21002
ACS Appl. Mater. Interfaces 2021, 13, 14458−14469

effect mediated by individual MNP in LF-AMF; schematic representation of the LF-AMF magnetic coils with indicating of their main parameters (Figure S14); schematic illustration of the magneto-mechanical effects mediated by individual MNP in the LF-AMF (Figure S15); (VI) Experimental study of the DNA duplex cleavage; and histograms of the sCy5 fluorescence intensity after treatment of duplexes (18−60 bp) formed using MNP-oligo-12 by the LF-AMF (f = 180 Hz, τ = 10 min) at various field amplitudes (Figure S16) (PDF)

AUTHOR INFORMATION

Corresponding Authors

Aleksey A. Nikitin − *National University of Science and Technology (MISIS), Moscow 119049, Russia; M. V. Lomonosov Moscow State University, Moscow 119991, Russia;* orcid.org/0000-0002-9183-6713; Email: nikitin.aa@misis.ru

Maxim A. Abakumov − *National University of Science and Technology (MISIS), Moscow 119049, Russia; Department of Medical Nanobiotechnology, N. I. Pirogov Russian National Research Medical University, Moscow 117997, Russia;* orcid.org/0000-0003-2622-9201; Email: abakumov_ma@rsmu.ru

Authors

Anton Yu Yurenya − *M. V. Lomonosov Moscow State University, Moscow 119991, Russia; National Research Center "Kurchatov Institute", Moscow 123098, Russia*

Timofei S. Zatsepin − *M. V. Lomonosov Moscow State University, Moscow 119991, Russia; Skolkovo Institute of Science and Technology, Moscow 121205, Russia;* orcid.org/0000-0003-0030-9174

Ilya O. Aparin − *Skolkovo Institute of Science and Technology, Moscow 121205, Russia;* orcid.org/0000-0001-8818-485X

Vladimir P. Chekhonin − *Department of Medical Nanobiotechnology, N. I. Pirogov Russian National Research Medical University, Moscow 117997, Russia*

Alexander G. Majouga − *National University of Science and Technology (MISIS), Moscow 119049, Russia; M. V. Lomonosov Moscow State University, Moscow 119991, Russia; D. Mendeleev University of Chemical Technology of Russia, Moscow 125047, Russia;* orcid.org/0000-0002-5184-5551

Michael Farle − *Faculty of Physics and Center for Nanointegration Duisburg-Essen, University of Duisburg-Essen, Duisburg 47057, Germany*

Ulf Wiedwald − *Faculty of Physics and Center for Nanointegration Duisburg-Essen, University of Duisburg-Essen, Duisburg 47057, Germany*

Complete contact information is available at: https://pubs.acs.org/10.1021/acsami.0c21002

Author Contributions

A.A.N. planned the experiments, prepared nanoparticles, and carried out experiments with magnetic field. A.Y.Y. performed XRD analysis, Mössbauer spectroscopy, and analyzed the data. T.S.Z. and I.O.A. designed and synthesized oligonucleotide sequences. V.P.C. and A.G.M. discussed the data and supervised all chemical experiments. M.F. analyzed and discussed the data. U.W. performed full magnetic characterization of the samples and analyzed the data. M.A.A. designed the study and coordinated the whole project. A.A.N., U.W., and M.A.A. wrote the manuscript with contributions from all authors who approved the submission.

Funding

The reported study was funded by RFBR according to the research project no. 19-03-00738 and by the Ministry of Science and Higher Education of the Russian Federation in the framework of Increase Competitiveness Program of NUST ≪MISiS≫ (grants no. K2A-2019-044 and K2-2020-029).

Notes

The authors declare no competing financial interest.

REFERENCES

(1) Kamau, S. W.; Hassa, P. O.; Steitz, B.; Petri-Fink, A.; Hofmann, H.; Hofmann-Amtenbrink, M.; von Rechenberg, B.; Hottiger, M. O. Enhancement of the Efficiency of Non-Viral Gene Delivery by Application of Pulsed Magnetic Field. *Nucleic Acids Res.* **2006**, *34*, No. e40.

(2) Zhang, E.; Kircher, M. F.; Koch, M.; Eliasson, L.; Goldberg, S. N.; Renström, E. Dynamic Magnetic Fields Remote-Control Apoptosis via Nanoparticle Rotation. *ACS Nano* **2014**, *8*, 3192−3201.

(3) Shen, Y.; Wu, C.; Uyeda, T. Q. P.; Plaza, G. R.; Liu, B.; Han, Y.; Lesniak, M. S.; Cheng, Y. Elongated Nanoparticle Aggregates in Cancer Cells for Mechanical Destruction with Low Frequency Rotating Magnetic Field. *Theranostics* **2017**, *7*, 1735−1748.

(4) Cheng, Y.; Muroski, M. E.; Petit, D. C. M. C.; Mansell, R.; Vemulkar, T.; Morshed, R. A.; Han, Y.; Balyasnikova, I. V.; Horbinski, C. M.; Huang, X.; Zhang, L.; Cowburn, R. P.; Lesniak, M. S. Rotating Magnetic Field Induced Oscillation of Magnetic Particles for in Vivo Mechanical Destruction of Malignant Glioma. *J. Controlled Release* **2016**, *223*, 75−84.

(5) Naud, C.; Thebault, C.; Carrière, M.; HOU, Y.; Morel, R.; Berger, F.; Dieny, B.; Joisten, H. Cancer Treatment by Magneto-Mechanical Effect of Particles, a Review. *Nanoscale Adv.* **2020**, *2*, 3632−3655.

(6) Lin, Y. R.; Chan, C. H.; Lee, H. T.; Cheng, S. J.; Yang, J. W.; Chang, S. J.; Lin, S. F.; Chen, G. Y. Remote Magnetic Control of Autophagy in Mouse B-Lymphoma Cells with Iron Oxide Nanoparticles. *Nanomaterials* **2019**, *9*, 551.

(7) Huang, H.; Delikanli, S.; Zeng, H.; Ferkey, D. M.; Pralle, A. Remote Control of Ion Channels and Neurons through Magnetic-Field Heating of Nanoparticles. *Nat. Nanotechnol.* **2010**, *5*, 602−606.

(8) Knecht, L. D.; Ali, N.; Wei, Y.; Hilt, J. Z.; Daunert, S. Nanoparticle-Mediated Remote Control of Enzymatic Activity. *ACS Nano* **2012**, *6*, 9079−9086.

(9) Tiwari, A. P.; Ghosh, S. J.; Pawar, S. H. Biomedical Applications Based on Magnetic Nanoparticles:DNA Interactions. *Anal. Methods* **2015**, *7*, 10109−10120.

(10) Moerland, C. P.; Van IJzendoorn, L. J.; Prins, M. W. J. Rotating Magnetic Particles for Lab-on-Chip Applications-a Comprehensive Review. *Lab Chip* **2019**, *19*, 919−933.

(11) Lauback, S.; Mattioli, K. R.; Marras, A. E.; Armstrong, M.; Rudibaugh, T. P.; Sooryakumar, R.; Castro, C. E. Real-Time Magnetic Actuation of DNA Nanodevices via Modular Integration with Stiff Micro-Levers. *Nat. Commun.* **2018**, *9*, No. 1446.

(12) Neuman, K. C.; Nagy, A. Single-Molecule Force Spectroscopy: Optical Tweezers, Magnetic Tweezers and Atomic Force Microscopy. *Nat. Methods* **2008**, *5*, 491−505.

(13) Kilinc, D.; Lee, G. U. Advances in Magnetic Tweezers for Single Molecule and Cell Biophysics. *Integr. Biol.* **2014**, *6*, 27−34.

(14) Danilowicz, C.; Greenfield, D.; Prentiss, M. Dissociation of Ligand-Receptor Complexes Using Magnet Tweezers. *Anal. Chem.* **2005**, *77*, 3023−3028.

(15) Mosconi, F.; Allemand, J. F.; Croquette, V. Soft Magnetic Tweezers: A Proof of Principle. *Rev. Sci. Instrum.* **2011**, *82*, No. 034302.
(16) Oberstrass, F. C.; Fernandes, L. E.; Bryant, Z. Torque Measurements Reveal Sequence-Specific Cooperative Transitions in Supercoiled DNA. *Proc. Natl. Acad. Sci. U.S.A.* **2012**, *109*, 6106−6111.
(17) Kolhatkar, A. G.; Jamison, A. C.; Litvinov, D.; Willson, R. C.; Lee, T. R. Tuning the Magnetic Properties of Nanoparticles. *Int. J. Mol. Sci.* **2013**, *14*, 15977−16009.
(18) Li, X.; Lu, W.; Song, Y.; Wang, Y.; Chen, A.; Yan, B.; Yoshimura, S.; Saito, H. Quantitatively Probing the Magnetic Behavior of Individual Nanoparticles by an AC Field-Modulated Magnetic Force Microscopy. *Sci. Rep.* **2016**, *6*, No. 22467.
(19) Etoc, F.; Lisse, D.; Bellaiche, Y.; Piehler, J.; Coppey, M.; Dahan, M. Subcellular Control of Rac-GTPase Signalling by Magnetogenetic Manipulation inside Living Cells. *Nat. Nanotechnol.* **2013**, *8*, 193−198.
(20) Seo, D.; Southard, K. M.; Kim, J. W.; Lee, H. J.; Farlow, J.; Lee, J. U.; Litt, D. B.; Haas, T.; Alivisatos, A. P.; Cheon, J.; Gartner, Z. J.; Jun, Y. W. A Mechanogenetic Toolkit for Interrogating Cell Signaling in Space and Time. *Cell* **2016**, *165*, 1507−1518.
(21) Lee, J. H.; Kim, J. W.; Levy, M.; Kao, A.; Noh, S. H.; Bozovic, D.; Cheon, J. Magnetic Nanoparticles for Ultrafast Mechanical Control of Inner Ear Hair Cells. *ACS Nano* **2014**, *8*, 6590−6598.
(22) Zablotskii, V.; Lunov, O.; Dejneka, A.; Jastrabk, L.; Polyakova, T.; Syrovets, T.; Simmet, T. Nanomechanics of Magnetically Driven Cellular Endocytosis. *Appl. Phys. Lett.* **2011**, *99*, No. 183701.
(23) Desprat, N.; Supatto, W.; Pouille, P. A.; Beaurepaire, E.; Farge, E. Tissue Deformation Modulates Twist Expression to Determine Anterior Midgut Differentiation in Drosophila Embryos. *Dev. Cell* **2008**, *15*, 470−477.
(24) Tseng, P.; Judy, J. W.; Di Carlo, D. Magnetic Nanoparticle-Mediated Massively Parallel Mechanical Modulation of Single-Cell Behavior. *Nat. Methods* **2012**, *9*, 1113−1119.
(25) Mannix, R. J.; Kumar, S.; Cassiola, F.; Montoya-Zavala, M.; Feinstein, E.; Prentiss, M.; Ingber, D. E. Nanomagnetic Actuation of Receptor-Mediated Signal Transduction. *Nat. Nanotechnol.* **2008**, *3*, 36−40.
(26) Ma, V. P. Y.; Salaita, K. DNA Nanotechnology as an Emerging Tool to Study Mechanotransduction in Living Systems. *Small* **2019**, *15*, No. e1900961.
(27) Kufer, S. K.; Puchner, E. M.; Gumpp, H.; Liedl, T.; Gaub, H. E. Single-Molecule Cut-and-Paste Surface Assembly. *Science* **2008**, *319*, 594−596.
(28) Zuker, M. Mfold Web Server for Nucleic Acid Folding and Hybridization Prediction. *Nucleic Acids Res.* **2003**, *31*, 3406−3415.
(29) Efremova, M. V.; Nalench, Y. A.; Myrovali, E.; Garanina, A. S.; Grebennikov, I. S.; Gifer, P. K.; Abakumov, M. A.; Spasova, M.; Angelakeris, M.; Savchenko, A. G.; Farle, M.; Klyachko, N. L.; Majouga, A. G.; Wiedwald, U. Size-Selected Fe3O4-Au Hybrid Nanoparticles for Improved Magnetism-Based Theranostics. *Beilstein J. Nanotechnol.* **2018**, *9*, 2684−2699.
(30) Kuerbanjiang, B.; Wiedwald, U.; Haering, F.; Biskupek, J.; Kaiser, U.; Ziemann, P.; Herr, U. Exchange Bias of Ni Nanoparticles Embedded in an Antiferromagnetic IrMn Matrix. *Nanotechnology* **2013**, *24*, No. 455702.
(31) Liébana-Viñas, S.; Wiedwald, U.; Elsukova, A.; Perl, J.; Zingsem, B.; Semisalova, A. S.; Salgueiriño, V.; Spasova, M.; Farle, M. Structure-Correlated Exchange Anisotropy in Oxidized Co80Ni20 Nanorods. *Chem. Mater.* **2015**, *27*, 4015−4022.
(32) Marko, J. F.; Cocco, S. The Micromechanics of DNA. *Phys. World* **2003**, *16*, 37−41.
(33) Meister, M. Physical Limits to Magnetogenetics. *eLife* **2016**, *5*, No. e17210.
(34) Golovin, Y. I.; Gribanovsky, S. L.; Golovin, D. Y.; Klyachko, N. L.; Majouga, A. G.; Master, A. M.; Sokolsky, M.; Kabanov, A. V. Towards Nanomedicines of the Future: Remote Magneto-Mechanical Actuation of Nanomedicines by Alternating Magnetic Fields. *J. Controlled Release* **2015**, *219*, 43−60.
(35) Dutz, S.; Hergt, R. Magnetic Particle Hyperthermia - A Promising Tumour Therapy? *Nanotechnology* **2014**, *25*, No. 452001.
(36) Pablico-Lansigan, M. H.; Situ, S. F.; Samia, A. C. S. Magnetic Particle Imaging: Advancements and Perspectives for Real-Time in Vivo Monitoring and Image-Guided Therapy. *Nanoscale* **2013**, *5*, 4040−4055.
(37) Gazeau, F.; Lévy, M.; Wilhelm, C. Optimizing Magnetic Nanoparticle Design for Nanothermotherapy. *Nanomedicine* **2008**, *3*, 831−844.
(38) Ota, S.; Takemura, Y. Characterization of Néel and Brownian Relaxations Isolated from Complex Dynamics Influenced by Dipole Interactions in Magnetic Nanoparticles. *J. Phys. Chem. C* **2019**, *123*, 28859−28866.
(39) Bellizzi, G.; Bucci, E. M.; Bucci, O. M. Analysis and Design of Magnetically Driven Nanomachines. *IEEE Trans. Nanotechnol.* **2011**, *10*, 1131−1140.
(40) Pope, L. H.; Davies, M. C.; Laughton, C. A.; Roberts, C. J.; Tendler, S. J. B.; Williams, P. M. Force-Induced Melting of a Short DNA Double Helix. *Eur. Biophys. J.* **2001**, *30*, 53−62.
(41) Strunz, T.; Oroszlan, K.; Schäfer, R.; Güntherodt, H. J. Dynamic Force Spectroscopy of Single DNA Molecules. *Proc. Natl. Acad. Sci. U.S.A.* **1999**, *96*, 11277−11282.
(42) Bustamante, C.; Bryant, Z.; Smith, S. B. Ten Years of Tension: Single-Molecule DNA Mechanics. *Nature* **2003**, *421*, 423−427.
(43) Bryant, Z.; Stone, M. D.; Gore, J.; Smith, S. B.; Cozzarelli, N. R.; Bustamante, C. Structural Transitions and Elasticity from Torque Measurements on DNA. *Nature* **2003**, *424*, 338−341.
(44) Forth, S.; Deufel, C.; Sheinin, M. Y.; Daniels, B.; Sethna, J. P.; Wang, M. D. Abrupt Buckling Transition Observed during the Plectoneme Formation of Individual DNA Molecules. *Phys. Rev. Lett.* **2008**, *100*, No. 148301.
(45) Lipfert, J.; Kerssemakers, J. W. J.; Jager, T.; Dekker, N. H. Magnetic Torque Tweezers: Measuring Torsional Stiffness in DNA and RecA-DNA Filaments. *Nat. Methods* **2010**, *7*, 977−980.
(46) Ho, D.; Zimmermann, J. L.; Dehmelt, F. A.; Steinbach, U.; Erdmann, M.; Severin, P.; Falter, K.; Gaub, H. E. Force-Driven Separation of Short Double-Stranded DNA. *Biophys. J.* **2009**, *97*, 3158−3167.
(47) Gao, L.; Wu, J.; Gao, D.; Wu, J. Separation of Long DNA Molecules through Cleavage of Hydrogen Bonds under a Stretching Force. *Appl. Phys. Lett.* **2007**, *91*, No. 113902.
(48) Ackerson, C. J.; Sykes, M. T.; Kornberg, R. D. Defined DNA/Nanoparticle Conjugates. *Proc. Natl. Acad. Sci. U.S.A.* **2005**, *102*, 13383−13385.
(49) Claridge, S. A.; Liang, H. W.; Basu, S. R.; Fréchet, J. M. J.; Alivisatos, A. P. Isolation of Discrete Nanoparticle-DNA Conjugates for Plasmonic Applications. *Nano Lett.* **2008**, *8*, 1202−1206.
(50) Riedinger, A.; Guardia, P.; Curcio, A.; Garcia, M. A.; Cingolani, R.; Manna, L.; Pellegrino, T. Subnanometer Local Temperature Probing and Remotely Controlled Drug Release Based on Azo-Functionalized Iron Oxide Nanoparticles. *Nano Lett.* **2013**, *13*, 2399−2406.
(51) Rutkauskas, M.; Krivoy, A.; Szczelkun, M. D.; Rouillon, C.; Seidel, R. Single-Molecule Insight Into Target Recognition by CRISPR−Cas Complexes. *Methods Enzymol.* **2017**, *582*, 239−273.
(52) Farzan, V. M.; Ulashchik, E. A.; Martynenko-Makaev, Y. V.; Kvach, M. V.; Aparin, I. O.; Brylev, V. A.; Prikazchikova, T. A.; Maklakova, S. Y.; Majouga, A. G.; Ustinov, A. V.; Shipulin, G. A.; Shmanai, V. V.; Korshun, V. A.; Zatsepin, T. S. Automated Solid-Phase Click Synthesis of Oligonucleotide Conjugates: From Small Molecules to Diverse N-Acetylgalactosamine Clusters. *Bioconjugate Chem.* **2017**, *28*, 2599−2607.
(53) Nikitin, A.; Fedorova, M.; Naumenko, V.; Shchetinin, I.; Abakumov, M.; Erofeev, A.; Gorelkin, P.; Meshkov, G.; Beloglazkina, E.; Ivanenkov, Y.; Klyachko, N.; Golovin, Y.; Savchenko, A.; Majouga, A. Synthesis, Characterization and MRI Application of

Magnetite Water-Soluble Cubic Nanoparticles. *J. Magn. Magn. Mater.* **2017**, *441*, 6−13.
(54) Huang, D.; Zhou, H.; Gao, J. Nanoparticles Modulate Autophagic Effect in a Dispersity-Dependent Manner. *Sci. Rep.* **2015**, *5*, No. 14361.
(55) Kibbe, W. A. OligoCalc: An Online Oligonucleotide Properties Calculator. *Nucleic Acids Res.* **2007**, *35*, W43−W46.

https://doi.org/10.1021/acsami.0c21002
ACS Appl. Mater. Interfaces 2021, 13, 14458−14469